Materials Research. 2024; 27:e20230451
DOI: https://doi.org/10.1590/1980-5373-MR-2023-0451

The Control of Flow Localization in the Post Severe Plastic Deformation (SPD) Forming of Aluminum Through the Application of Low Strain Amplitude Multidirectional (LSA-MDF) Forging

C.G. de Faria[a,b], *M.T.P. Aguilar*[c], *P.R. Cetlin*[d*]

[a]*Universidade Federal de Minas Gerais, Programa de Pós-Graduação em Engenharia Metalúrgica, Materiais e de Minas, Belo Horizonte, MG, Brasil.*
[b]*Newton Paiva - Centro Universitário, Belo Horizonte, MG, Brasil.*
[c]*Universidade Federal de Minas Gerais, Departamento de Engenharia de Materiais e Construção, Belo Horizonte, MG, Brasil.*
[d]*Universidade Federal de Minas Gerais, Departamento de Engenharia Mecânica, Belo Horizonte, MG, Brasil.*

Received: October 16, 2023; Revised: March 20, 2024; Accepted: April 24, 2024

Severe Plastic Deformation (SPD) of metals leads to their strengthening and losses in the work hardening capacity. The latter causes flow localization upon subsequent forming of the material. The application of Low Strain Amplitude Multi-Directional Forging (LSA-MDF) after SPD regenerates the material work hardening capacity and available results cover 4LSA-MDF cycles after 1 and 4ECAP (Equal Channel Angular Pressing) passes in aluminum; the effect of more LSA-MDF cycles after ECAP is not known. This paper presents results for the application of 8, 12 and 16LSA-MDF cycles after 4ECAP passes in aluminum, which led to further work hardening capacity regeneration of the material. The corresponding microstructural evolution involved an increase and stabilization of the HAGBs fraction and increases in the 5-15º boundary disorientation fraction. Monotonic compression after ECAP+LSA-MDF exhibited almost linear work hardening rates, connected to decreases in the HAGBs fraction and increases in the 2-5º boundary disorientation fraction.

Keywords: *Aluminum, Severe Plastic Deformation, Low Strain Amplitude Multi-Directional Forging, Microstructures, Work hardening.*

1. Introduction

Severe Plastic Deformation (SPD) of metals imposes high levels of cold plastic deformation on the material without significant changes in the initial shape and dimensions of the specimens[1] and has received wide scientific attention in the last decades[2]. SPD leads to grain refinement of the materials down to the nanometric scale (Ultra-Fine Grains, UFG)[3,4] and thus to their remarkable strengthening[5], as well as to their superplastic behavior under high strain rates and adequate temperature ranges[6].

The most frequently employed SPD techniques are High Pressure Torsion (HPT)[7,8], Equal Channel Angular Pressing (ECAP)[9] and Multi-Directional Forging (MDF)[10], also known as Multi-Axial Forging (MAF)[11] or Multi-Axial Compression (MAC)[12]. HPT requires specialized equipment and usually supplies cylindrical or tubular specimens. Inversions of the torsion direction allow the application of cyclic HPT with any desired straining amplitude ($\Delta\varepsilon$)[13]. ECAP is widely utilized, can be adapted to continuous production and to large specimens, exhibits high friction between the material and the dies and problems such as plastic instabilities, cracks and specimen segmentation in the processing of difficult-to-work materials[14]. MDF involves successive identical compressions with a deformation amplitude $\Delta\varepsilon$ along the three orthogonal axes of cuboid specimens[15], can be applied to large (industrial) workpieces employing any testing machine or industrial press and allows the evaluation of the *in-situ* stress-strain characteristics of the material during processing[10,16,17]. Free MDF compressions cause specimen distortions, whose elimination demands the use of various constraining dies[18]. MDF allows the use of various strain amplitudes $\Delta\varepsilon$.

Although SPD remarkably strengthens materials and refines their grains, post SPD monotonic deformation exhibits low or negative work hardening, as reported, for example, by Beyerlein et al.[19] for 99.99% aluminum and copper and by El-Danaf et al.[20] for 1050 aluminum. As a consequence, these materials may not perform well where necking or flow localization may occur during processing.

Diffuse and/or localized necks are triggered at low strains in the post SPD tension of materials; Considére's condition for neck inception $\left(\gamma' = (1/\bar{\sigma}).(d\bar{\sigma}/d\bar{\varepsilon})_{\dot{\varepsilon}}\right) < 1$, where $\bar{\sigma}$ and $\bar{\varepsilon}$ are the effective stress and effective strain respectively and $\dot{\varepsilon}$ is the effective strain rate, is reached at low strains due to the high levels of $\bar{\sigma}$, thus severely limiting sheet metal forming for SPD processed materials.

*e-mail: pcetlin@gmail.com

Flow localization occurs as concentrated deformation bands in important plane strain forming processes such as flat rolling and some forging and bar drawing processes[21], whenever the maximum value of the parameter $\alpha = (\gamma'/m)$ of the material rises above ≈ 5[22], where "m" is the material strain rate sensitivity and γ' is now calculated under work softening conditions. For example, according to data from El-Danaf et al.[20] for room temperature compression of 1050 UFG aluminum after 4 and 8 ECAP passes following route Bc, the flow stress drops from ≈ 175 MPa to ≈ 150 MPa for strains 0.1 and 1.3, respectively. Assuming a constant average softening rate of ≈ (175 – 150)/(1.3 – 0.1) ≈ 20.8 MPa in the strain interval, at the beginning of the softening $\gamma' = 20.8/175 \approx 0.12$. The strain rate sensitivity of this material at room temperature is m ≈ 0.014[23], and thus α ≈ 8.50 which is an indication that the material is susceptible to the flow localization and consequent deformation bands when processed under plane strain conditions. Accordingly, the authors reported that the softening is partly attributed to experimentally observed localized shear bands. Materials with limited ductility processed under plane strain with $\alpha_{max} > \approx 5$ may crack along the deformation bands. A possible example of such a situation is the axial compression after ECAP of a 7010AA aluminum alloy[24], where the material already exhibited localized flow regions after ECAP. Work softening was observed after a compression strain ≈ 0.1, followed by fractures along planar surfaces at 45º with the compressive stress, parallel to the same direction, even though compression was performed with a cylindrical sample (i. e. not under plane strain). Specimen segmentation during ECAP is also associated with the work-softening of the material[25]

Adiabatic heating aggravates flow localization phenomena, since it leads to an additional softening of the material as its temperature rises. On the other hand, work hardening eliminates or greatly alleviates flow localization phenomena and it is thus desirable in the post SPD processing of materials. Some techniques, involving microstructural and compositional aspects, have been suggested in order to reach this goal: i) a bi-modal grain size distribution[26-28] ii) the introduction of nano-precipitates in the material[29,30] and iii) high Zn contents in Aluminum[31].

A seminal study on the MDF processing of aluminum[32] showed that the strain amplitude (Δε) influences the work hardening of the annealed material, whose saturation flow stress is lowered as Δε decreases. Furthermore, it was shown that the application of Low Strain Amplitude MDF (LSA-MDF with Δε ≈ 0.075) after monotonic compression leads to a material softening where the flow stress tends to the saturation flow stress corresponding to processing with only LSA-MDF. Most important of all, if monotonic compression is applied after initial monotonic compression + LSA-MDF, the material displays a positive work hardening rate and tends to return to flow stress levels similar to those in purely monotonic compression. Such findings spurred recent studies by the authors, where 4LSA-MDF cycles (Δε ≈ 0.075, deformation ε ≈ 0.225 for each cycle of 3 compressions, total deformation after 4 cycles ε ≈ 0.9) were applied after 1 and 4ECAP passes (route Bc, Δε ≈ 1.15 in each pass, total strain after 4ECAP passes ε ≈ 4.6)[33,34] in commercial purity aluminum, followed by monotonic compression. The results were similar to those reported above by Armstrong et al.[32] above: LSA-MDF led to softening of the ECAPed material and to a regeneration of its work hardening capacity under subsequent monotonic compression. From the point of view of the control of flow localization of SPD processed material, such results are highly desirable.

The influence of strain amplitude (Δε) on the resulting saturation flow stress in cyclic HPT[13] is similar to that in MDF: decreasing Δε lowers the saturation stress. The reported results don't cover either cyclic torsion after monotonic torsion or monotonic torsion after cyclic torsion, but it is believed that the results would be similar to those reported above for MDF. Cyclic tension-compression of various metals also indicates the same effect of Δε on the saturation flow stress in MDF and cyclic HPT[35]. In addition, it was shown that cyclic tension-compression with a strain amplitude (Δε) lower than a previous monotonic deformation will lead to material softening down to the saturation flow stress corresponding to purely cyclic strain with the same strain amplitude. It has also been already shown that hot monotonic and cyclic torsion (with various strain amplitudes) of copper and IF steel in the austenitic range, as well as their successive application[36-39] lead to behaviors very similar to those already discussed by Armstrong et al.[32] above. It thus seems reasonable to conclude that these results, derived from LSA-MDF and simple compression may occur for various sequences of monotonic + LSA-cyclic/multiaxial + monotonic plastic deformation of metals.

Softening phenomena in SPD is an important aspect in the context of the present investigation. An extensive and recent review of the production of nano-structured materials through [SPD4] indicates that the flow stress of pure metals with low melting temperatures decreases and then saturates as applied strains rise. Metals with moderate melting temperatures such as pure Aluminum and Magnesium initially harden and then soften down to a steady state flow stress above that typical of materials with coarse grains, as already described in 1976 by Erbel; it is remarkable that ultra-high purity aluminum (99.9999% purity) softens to a stress level below that for a coarse grained material[40]. Materials with higher melting temperatures, as well as most alloys, display an increasing flow stress followed by its saturation as the applied SPD strain is raised; this would be the most frequent behavior of materials submitted to SPD.

Softening during SPD has been attributed to various phenomena: (i) solute precipitation during HPT processing of Al-Zn as cast alloys[41] (ii) a transition of the plastic deformation mechanism from a situation dominated by dislocation phenomena to grain boundary sliding, with an attendant increase in the material strain rate sensitivity and consequent high tensile elongations typical of superplasticity, as was shown for example for a Zn–Al–Cu–Mg hypoeutectic alloy processed by multi-directional forging at room temperature[42], (iii) formation of localized shear bands[20] (iv) Kapoor et al.[43] proposed that the initial hardening and subsequent softening of aluminum during MDF with Δε ≈ 0.78, occurring at a transition total deformation ε ≈ 5, is caused by an initial increase in the LAGBs fraction and in the dislocation density, followed by a transformation of the LAGBs into HAGBs, causing a decrease in the dislocation density and softening the material. A general analysis of this situation predicts that these hardening/softening transitions should be observed at total strains ε ≈ 2.5 - 4 for ECAP, HPT and ARB[44], but did not cover processing with MDF (v) other softening mechanisms would be related to dynamic recovery phenomena, continuous dynamic recrystallization, grain boundary controlled annihilation of dislocations and residual internal stresses[43].

The microstructural evolution of the material along the 1 and 4ECAP+4LSA-MDF + Compression procedures revealed that the post ECAP application of LSA-MDF caused an increase in the High Angle Grain Boundaries (HAGBs) fraction in the material as well as a decrease in the presence of distorted grains containing internal dislocation structures. In addition, the evolution of the dislocation structures associated with the application of LSA-MDF occurred at lower total strains when compared with the same the evolution caused only by deformation in ECAP[45,46]. The monotonic compression with a strain ε ≈ 0.8 after 4ECAP+4LSA-MDF cycles decreased the HAGBs fraction and increased the size of regions surrounded by HAGBs and their subdivision with Low Angle Grain Boundaries (LAGBs). Such findings are in line with the model described above Kapoor et al.[43] for the initial hardening and subsequent softening of aluminum during MDF with Δε ≈ 0.78. In the present situation, LSA-MDF would soften the material through a mechanically driven transformation of LAGBs into HAGBs; subsequent monotonic compression inverts this transformation, leading to a positive work hardening of the material.

Combinations of SPD deformation procedures have been used in order to enhance the grain refinement and thus the mechanical strength increase generated by SPD, such as ECAP + extrusion[47], MDF+ECAP+MDF[48], ECAP+cold rolling and ECAP+[HPT9]. No reference was found in the literature for the sequence ECAP+LSA-MDF, which does not aim at enhanced grain refinement through SPD.

The ECAP+LSA-MDF deformation route is of interest in order to obtain material displaying high strength coupled to appreciable work hardening capacity, leading to the control of localized flow phenomena especially during plane strain processing of the material after SPD. However, information is lacking regarding the (i) effect of the number of LSA-MDF cycles on the softening and work hardening regeneration in commercial purity aluminum and (ii) microstructural evolution of the material along the number of LSA-MDF cycles. The present paper presents this analysis for the application of up to 16LSA-MDF cycles (Δε ≈ 0.075) after 4ECAP passes along the Bc route (Δε ≈ 1.15, total strain ε ≈ 4.60). Finite element simulations of plane strain processing, considering the various measured work hardening behaviors measured in the present investigation, demonstrates the decrease in the localized flow for the material after ECAP+LSA-MDF, in comparison with the material submitted only to ECAP.

2. Material and Methods

The material was commercial purity cast aluminum (Al-99.77, Fe-0.15, Si-0.06 wt%) in cylinders 150 mm in diameter. Samples 15.8 x 15.8 x 100 mm were machined from this bar, with the long dimension parallel to the cylinder axis. These were initially deformed in 1ECAP pass with channels at 90º with no external curvature and dimensions 15.9 x 15.9 mm, imposing a strain Δε ≈ 1.15[49], at room temperature and at a speed of ≈ 20 mm/min; the die/specimen interface was lubricated with molybdenum disulfide. The deformed specimens were then annealed at 673 K for 7200 s and air cooled thus leading to the elimination of the initial as-cast microstructure. The annealed specimens were then submitted to 4ECAP passes with the same die and procedures above described, imposing a total strain ε ≈ 4.6, following route Bc[50].

MDF specimens were machined out of the ECAPed material, whose X direction was along the specimen axis, direction Z was parallel to the axial direction of the specimen before it underwent the deformation in the ECAP die and direction Y was orthogonal to directions X and [Z18]. The MDF specimens had the dimensions: 13.00 (direction X), 12.06 (direction Y) and 12.52 (direction Z) mm. Compressions at room temperature with a strain amplitude Δε ≈ 0.075, utilizing a confining die where the initial deformation occurs under simple compression18, followed the sequence of X, Z and Y directions. The interfaces between the compression die and the specimen were lubricated with molybdenum disulfide. For all compression steps, the direction under compression had (i) an initial length of 13.00 mm after the previous Δε ≈ 0.075 straining in an orthogonal direction, and (ii) underwent a decrease in length of 0.94 mm. MDF was performed for 8, 12 or 16LSA-MDF cycles (24, 36 and 48 compressions, total strains ε ≈ 1.8, 2.7 and 3.6 respectively).

Monotonic compression tests were performed after processing 4ECAP+8LSA-MDF, 4ECAP+12LSA-MDF and 4ECAP+16LSA-MDF cycles, along the X direction in the specimen up to a total strain of ε ≈ 0.8; testing was interrupted for every ε ≈ 0.1 increment for interface re-lubrication with molybdenum dissulfate paste.

All MDF and compression processing were performed in duplicate in an INSTRON 5582 universal testing machine, at a crosshead speed of ≈ 0.005 mm/s. No remarkable differences were observed when comparing the results obtained for both sets of specimens. The raw load versus displacement data from the mechanical testing were converted into true stress versus true strains considering the instantaneous height of the specimens and a constant volume, in order to calculate their average cross-section area.

The microstructural analyses involved Electron Backscattered Diffraction (EBSD) and Transmission Electron Microscopy (TEM) in the central region of the specimen cross-sections orthogonal to (i) the extrusion direction for 4ECAP (X direction), (ii) the first LSA-MDF compressed direction for the 8, 12 and 16LSA-MDF cycles (X direction), and (iii) the compression direction for uniaxial monotonic compressions. At least 2 different areas were analyzed for each processing condition; since no remarkable differences were observed between them, only one was chosen as typical for the present paper. A Quanta FEG 3D FEI SEM with a Bruker QUANTAX EBSD analysis system was utilized and data were processed with the ATEX software[51]. Disorientation detection of neighboring regions was set at an angle of 2º; the analyzed area in all cases was ≈ 1170 µm^2 and the step size was 50 nm. Noise elimination completed the absent indexing for some points through an averaging from neighboring points. Results were only accepted in case at least 85% of indexed points were covered. Whenever this level was not reached the data were discarded; an indexation level above 90% was commonly reached. Surface preparation for EBSD analyses involved an initial grinding with 400 mesh paper, electrolytic polishing (700 mL C_2H_5OH, 120 mL distilled H_2O, 100 mL $C_4H_9OC_2$- H_4OH, 68 mL-70% $HClO_4$ at 35 V for ≈ 45 s and a stainless steel cathode). TEM employed a Tecnai G2-20 SuperTwin FEI-200 kV; specimens were ground to a thickness of 100 µm, punched into 3 mm diameter discs and perforated with a double jet TENUPOL 5 using a 30% nitric acid–methanol solution at 243 K.

Finite element computational simulations of plane strain deformation of the post-SPD material was performed utilizing the QForm software; specimens were 60.0 mm long and 10.0 mm thick, compressed between dies 7.0 mm wide, displaying a 1.0 mm radius at their corners; compression speed was 0.2 mm/s. The initial relationship between specimen height (h) and die breadth (b) was thus h/b ≈ 1.43, causing flow localizations with a typical single "X" aspect[52]. Friction between the compression dies and the material causes the formation of restricted flow regions adjacent to the dies, inducing localized deformation around these regions. In order to allow the evaluation of the strain heterogeneity caused solely by a given plane strain geometry and the work hardening characteristics of the material, no friction was considered between the material and the dies. As a consequence, the strain heterogeneities obtained in the simulations will be less significant than when die/material friction is present, making the flow localization evaluation more stringent. The specimens were meshed with 15,000 elements (15,351 nodes). Time steps were taken as 0.01 s/step. Simulations were run till a true strain in the thickness direction $\varepsilon = 0.15$ was reached, corresponding to an effective strain $\bar{\varepsilon} = 1.15 \times 0.15 = 0.173$.

3. Results and Discussion

3.1. Mechanical aspects

Figure 1 displays the stress-strain curves for all the LSA-MDF steps after 4ECAP, as well as the monotonic compression curves after 4ECAP+8, 12 and 16LSA-MDF cycles. Data for compression after 4ECAP, after 4ECAP+4LSA-MDF and for the stress-strain curves for the initial 4LSA-MDF steps were taken from a previous publication[45]. All the stress-strain curves are similar to those previously reported[45], displaying rising stress levels after the specimens touched the confining die walls. An approximate envelope of the individual stress-strain curves for the stress at the beginning of this rise is shown.

The stress-strain curves for the monotonic compression after 4ECAP displays an initial work softening followed by a slow work hardening. On the other hand, the corresponding curves after 4ECAP+8, 12 and 16LSA-MDF cycles exhibited hardening with approximately linear rates ($\Delta\sigma/\Delta\varepsilon$), similarly to compression after 4ECAP+4LSA-MDF[45].

Considering the stress envelope in Figure 1, a softening of the material is observed from a flow stress ≈ 160MPa after 4ECAP down to ≈ 128 MPa (≈ 20% softening), ≈ 110 MPa (≈ 31.3% softening), ≈ 102 MPa (≈ 36.3% softening) and ≈ 100 MPa (≈ 37.5% softening) after 4, 8, 12, and 16LSA-MDF respectively. The softening rate decreases as LSA-MDF strain progresses, similarly to that described by Armstrong et al.[32] for the LSA-MDF of aluminum after monotonic compression and by Coffin and Tavernelli[53] for LSA cyclic tension/compression after monotonic straining of various materials.

The approximately linear work hardening displayed in the compression stress-strain curves differs from the usual parabolic hardening associated with dynamic recovery[54], suggesting that dislocation density and structures did not tend to equilibrium with dynamic recovery phenomena during the compression with strain $\varepsilon \approx 0.8$. Table 1 displays the average work hardening rates of the stress-strain curves in the final monotonic compression step for the various specimen conditions, as well as the final flow stress attained at the end of the monotonic compression. It can be seen that the work hardening rate rises as the number of LSA-MDF cycles increases, associated with small increases in the final compression flow stress.

Finite element simulations were performed for three material constitutive behaviors: (i) compression after 4ECAP and supposing no work hardening of the material

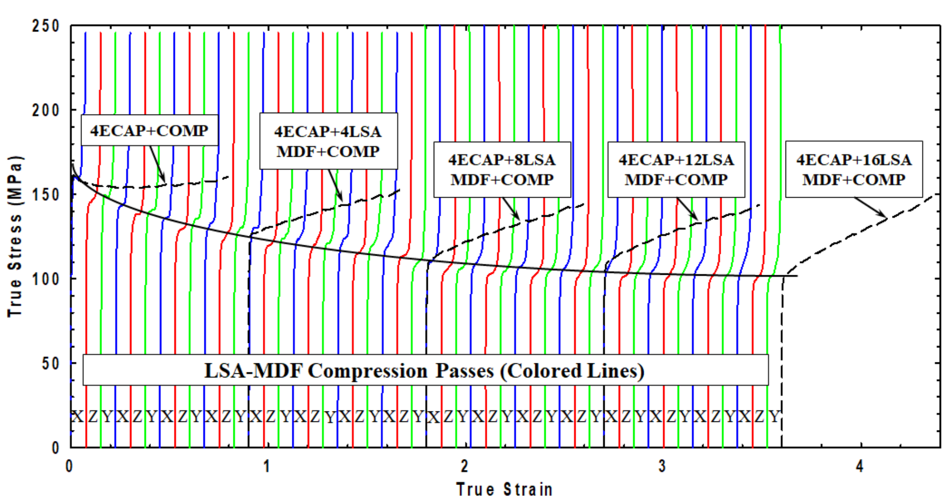

Figure 1. True stress - strain curves for compressions after 4ECAP, 4ECAP + 4, 8, 12 and 16LSA-MDF, and for all LSA-MDF steps.

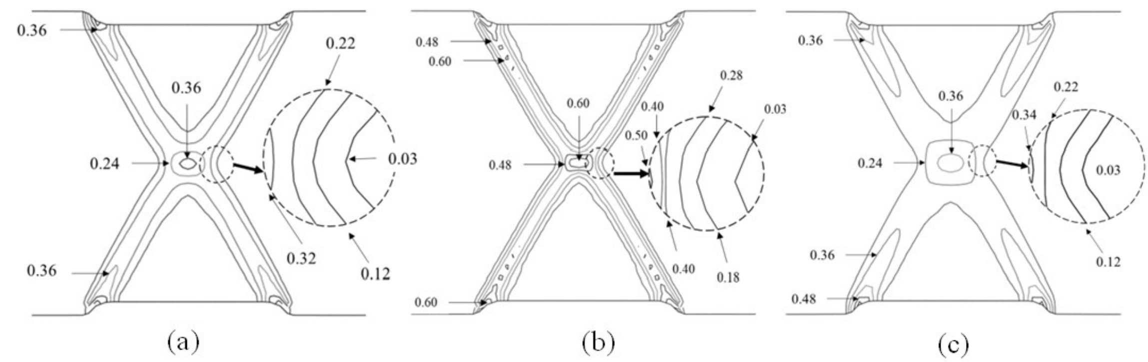

Figure 2. Effective strain ($\bar{\varepsilon}$) distributions after plane strain compression of the material for constitutive equations (a) $\bar{\sigma}$ = 160 MPa. (b) $\bar{\sigma}$ = 160 - 10 $\bar{\varepsilon}$ MPa and (c) $\bar{\sigma}$ = 104 + 42.5. $\bar{\varepsilon}$ MPa.

Table 1. Work hardening rates and flow stresses at the end of the monotonic compression step for the various specimen conditions.

Specimen condition	Work hardening rate under compression (MPa)	Flow stress at the end of the compression (MPa)
4ECAP+4LSA-MDF	30.0	152
4ECAP+8LSA-MDF	42.5	144
4ECAP+12LSA-MDF	52.5	144
4ECAP+16LSA-MDF	62.5	150

($\bar{\sigma}$ = 160 MPa), which corresponds to an "average" behavior of the material, (ii) compression after 4ECAP and accepting a softening rate where $\Delta\bar{\sigma}/\Delta\bar{\varepsilon}$ = -10 MPa ($\bar{\sigma}$ = 160 – 10. $\bar{\varepsilon}$ MPa), approximately corresponding to the initial softening rate of the $\bar{\sigma}$ versus $\bar{\varepsilon}$ curve after 4ECAP and (iii) compression after 4ECAP+8LSA-MDF ($\bar{\sigma}$ = 104 + 38. $\bar{\varepsilon}$ MPa), as typical of the hardening after ECAP+LSA-MDF.

Figure 2 shows the results for the effective strain ($\bar{\varepsilon}$) distribution in a plane strain compression computer simulation, displaying the expected strain localizations with an "X" shape. The comparison of Figures 2a and 2b indicates that the work softening at the beginning of the compression after ECAP leads not only to more flow localization, but also to higher levels of effective strains, whose values at the center of the specimen is raised from 0.36 to 0.60 when work softening is considered. The examination of Figure 2c reveals that the prevailing work hardening led to less flow localization. This confirms the importance of work hardening in order to avoid pronounced flow localizations in the plane strain processing of metals.

The envelope of the stress-strain curve for the first 4LSA-MDF cycles in Figure 1 displays a softening rate of (160 – 128)/0.9 MPa ≈ 35.5 MPa, leading to a value of the α parameter with a minimum value given by (35.5/160)/0.014 ≈ 15.8. Compression of the material under such circumstances will lead to pronounced flow localization and consequent specimen distortions under free compression. This has been experimentally observed and the situation can be circumvented with the use of confining dies, as covered in previous publications by the authors[18].

3.2. Dislocation structures

Figure 3 exhibits the Orientation Imaging Maps (OIM) extracted from the EBSD analyses for all experimental conditions in the present investigation; in addition, previously reported EBSD results for 4ECAP, 4ECAP+4LSA-MDF, 4ECAP+compression and 4ECAP+4LSA-MDF+Compression (hereafter the compression testing will be indicated by "COMP")[45] are also presented, in order to allow a broader view of the microstructural effects of the application of various numbers of LSA-MDF cycles after SPD. Black lines in all images in Figure 3 correspond to HAGBs whose disorientation across the boundaries exceeds 15º[55]. Figure 4 displays the grain boundary characteristics and disorientation values in the material for the same conditions in Figure 3. The various color lines indicate the disorientation ranges for the LAGBs (red for the 2º to 5º range, green for the 5º to 15º range) and blue for the HAGBs (boundaries with disorientations above 15º).

Figure 5 shows TEM images for the processing conditions discussed in this paper. The application of LSA-MDF after 4ECAP leads to structures with regions displaying limited internal dislocation structures, as can be seen through Figures 5a, 5b, 5e, 5f and 5g; monotonic compression after ECAP+LSA-MDF is connected to the presence of regions exhibiting internal dislocations structures (indicated, for example, by black arrows in in Figure 5j) and frequently distorted boundaries. Typical regions with tangled dislocation structures are indicated by the white arrows in Figure 5g.

Figures 6, 7 and 8 display the evolution of the percent fraction of HAGBs, LAGBs (5–15º disorientation) and LAGBs (2–5º disorientation), respectively, after 4 ECAP, 4 ECAP+4, 8, 12 and 16LSA-MDF cycles and for the compression after these LSA-MDF cycles. Data were taken from Figure 4 and from previous experiments[46] for the application of 4LSA-MDF and compression after 1 ECAP pass. Data for compression after 8 ECAP passes[20] were also included.

The overall shape of the curve for the HAGBs fraction versus $\bar{\varepsilon}$ curve (Figure 6) indicates an initial decrease of this fraction followed by its increase and stabilization for higher values of $\bar{\varepsilon}$ (a fraction ≈ 60% in the present case). Such shape is commonly observed and has been modeled for SPD generated by ECAP, ARB and HPT[44]. LSA-MDF

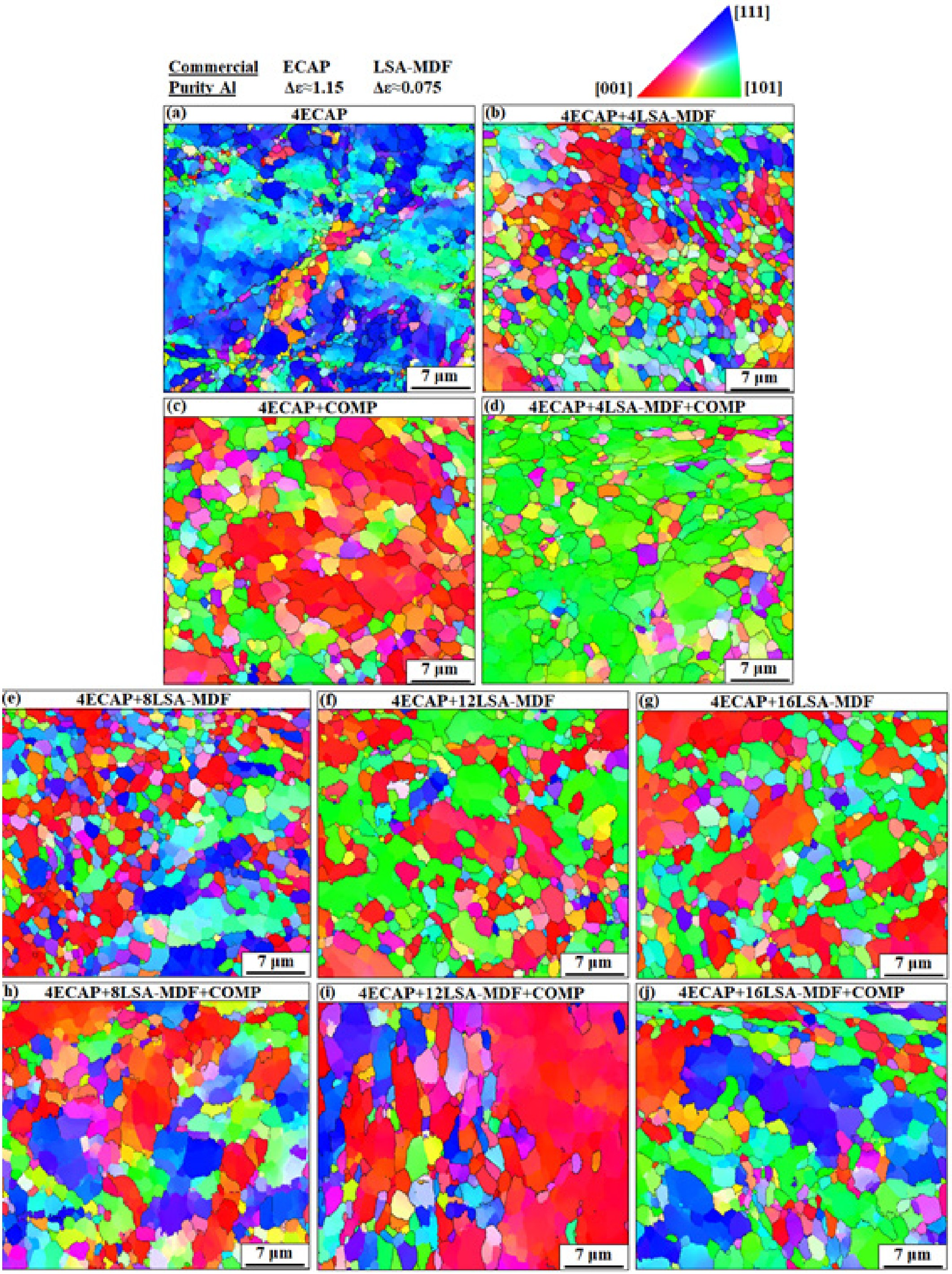

Figure 3. OIM for the conditions in the present investigation: (a) 4ECAP, (b) 4ECAP+4LSA-MDF, (c) 4ECAP+COMP, (d) 4ECAP+4LSA-MDF+COMP, (e) 4ECAP+8LSA-MDF, (f) 4ECAP+12LSA-MDF, (g) 4ECAP+16LSA-MDF, (h) 4ECAP+8LSA-MDF+COMP, (i) 4ECAP+12LSA-MDF+COMP e (j) 4ECAP+16LSA-MDF+COMP.

after both 1 and 4ECAP increases the measured HAGBs fractions to values above the expected levels for processing only with ECAP, whereas monotonic compression after LSA-MDF decreases these fractions to values below those expected from processing only with ECAP. Softening after 1 and 4ECAP is thus associated with increases in the HAGBs fraction, whereas the observed linear hardening in compression after ECAP + LSA-MDF is connected to decreases in the HAGBs fraction.

Data for direct compression after 8ECAP causes a pronounced decrease in the HAGBs fraction. It is however noteworthy that, whereas compression after LSA-MDF occurs with positive work hardening, the compression after 8ECAP involved softening that has been partly attributed to

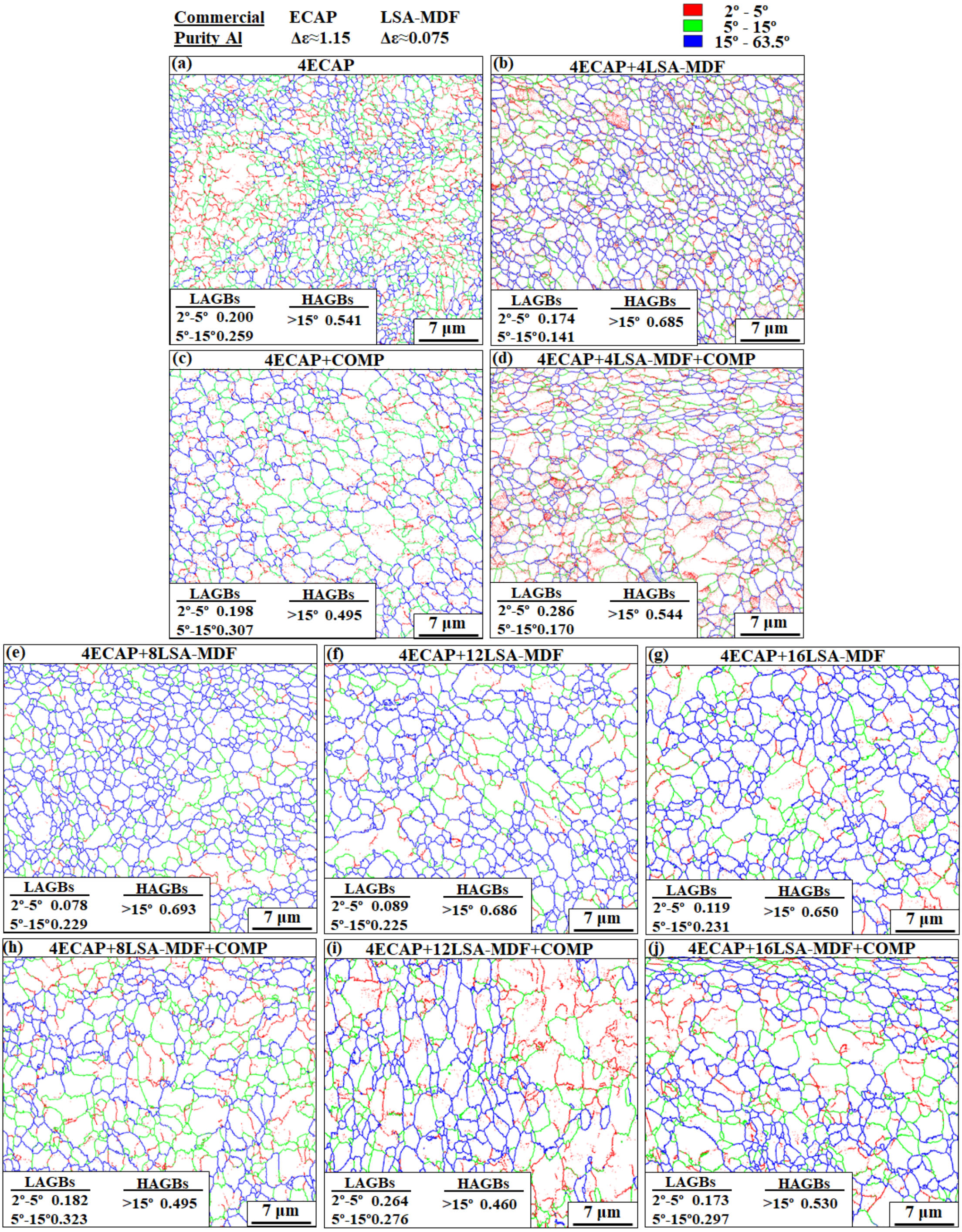

Figure 4. Grain boundary characteristics for the conditions in the present investigation: (a) 4ECAP, (b) 4ECAP+4LSA-MDF, (c) 4ECAP+COMP, (d) 4ECAP+4LSA-MDF+COMP, (e) 4ECAP+8LSA-MDF, (f) 4ECAP+12LSA-MDF, (g) 4ECAP+16LSA-MDF, (h) 4ECAP+8LSA-MDF+COMP, (i) 4ECAP+12LSA-MDF+COMP e (j) 4ECAP+16LSA-MDF+COMP.

the observed localized shear band formation[20], caused by an intrinsic softening of the material. The effective strain ($\bar{\varepsilon}$) distributions displayed in Figure 2 indicate the importance of a positive work hardening in order to avoid pronounced flow localizations during plane strain processing in the post-SPD deformation of materials. It is concluded that the initial dislocation structure in the material before its compression has a profound influence on its work hardening/softening response.

The decrease in the HAGBs fraction after 1ECAP is attributed to a pronounced increase in the LAGBs (2–5º) fraction, since the LAGBs (5-15º) fraction remains stable (see Figures 7 and 8). The rise in flow stress caused by 1ECAP is thus connected to the transformation of HAGBs into LAGBs

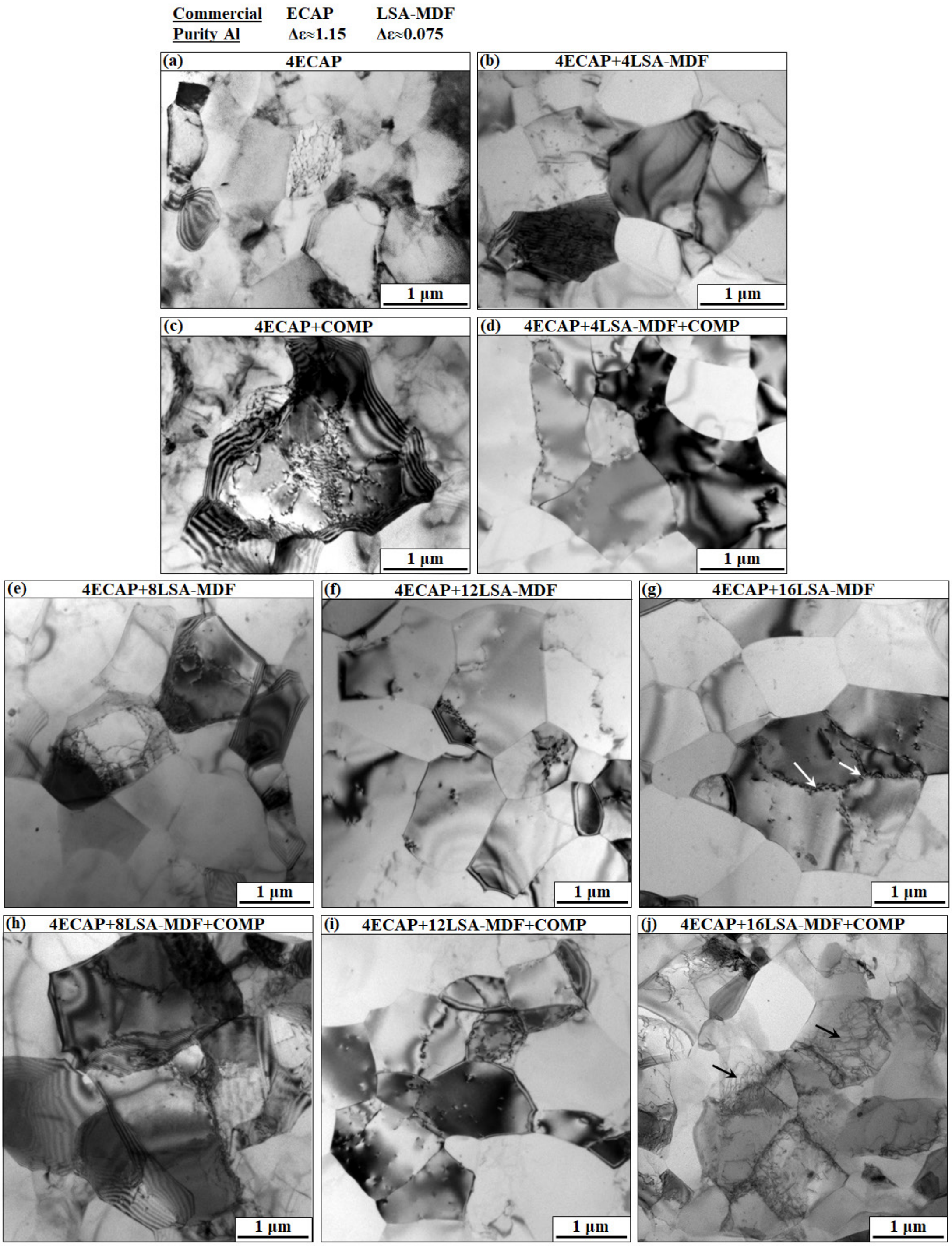

Figure 5. TEM images of the material after: (a) 4ECAP, (b) 4ECAP+4LSA-MDF, (c) 4ECAP+COMP, (d) 4ECAP+4LSA-MDF+COMP, (e) 4ECAP+8LSA-MDF, (f) 4ECAP+12LSA-MDF, (g) 4ECAP+16LSA-MDF, (h) 4ECAP+8LSA-MDF+COMP, (i) 4ECAP+12LSA-MDF+COMP and (j) 4ECAP+16LSA-MDF+COMP. Black arrows in in Figure 5j show examples of regions exhibiting internal dislocation structures; white arrows in Figure 5g indicates examples of regions with tangled dislocations.

(2-5º). The application of 4LSA-MDF cycles after 1 ECAP causes an increase in the HAGBs fraction, a small increase in the LAGBs (5-15º) fraction and a larger decrease in the LAGBs fraction (2-5º); the observed softening thus seems to be due to transformation of LAGBs (2-5º) into LAGBs (5-15º) and the evolution of the latter into HAGBs. The final compression after an increasing number of LSA-MDF cycles causes decreases in the HAGBs fraction and increases in both the LAGBs (5-15º) and LAGBs (2-5º), leading to the linear work hardening shown in Figure 1.

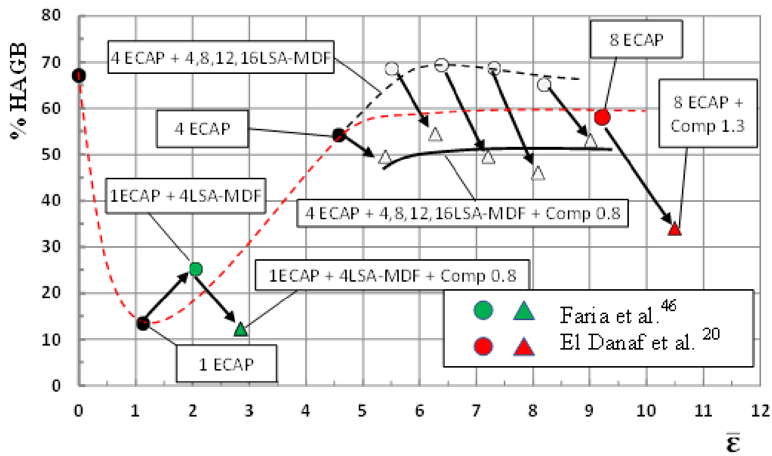

Figure 6. Variation of the percent fraction of HAGBs with the effective strain ($\bar{\varepsilon}$) for the application of LSA-MDF cycles and compression after ECAP and compression directly after ECAP.

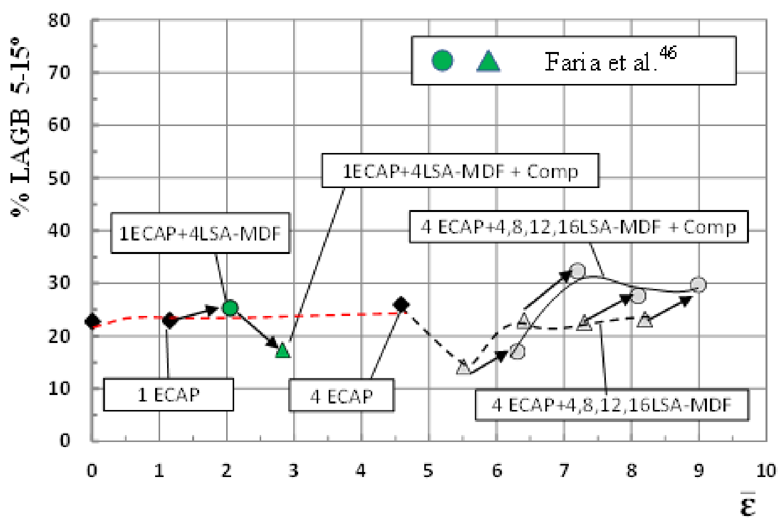

Figure 7. Variation of the percent fraction of LAGBs (5 – 15º disorientation) with the effective strain ($\bar{\varepsilon}$) for the application of LSA-MDF cycles and compression after ECAP.

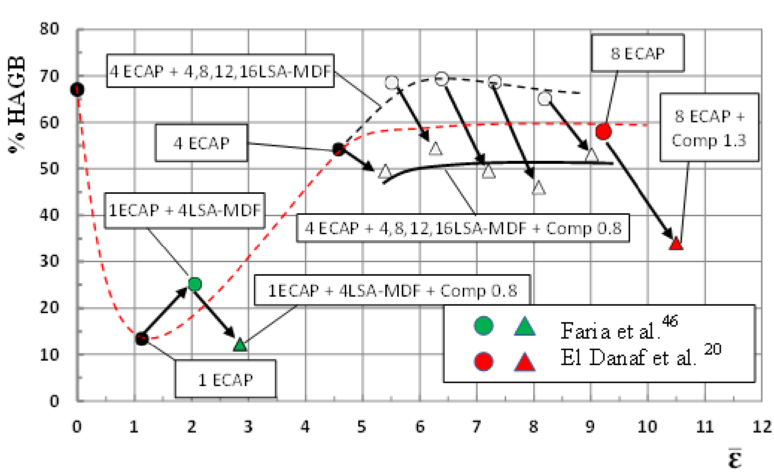

Figure 8. Variation of the percent fraction of LAGBs (2 – 5º disorientation) with the effective strain ($\bar{\varepsilon}$) for the application of LSA-MDF cycles and compression after ECAP.

The consideration of the above discussed evolution of the HAGBs, LAGBs (5-15º) and LAGBs (2-5º) supports the model proposed by Kapoor et al.[43]: as the strain imposed by SPD rises, one initially has the development of a “hard” dislocation structure corresponding to LAGBs and dislocation tangles, causing a strong hardening of the material; as deformation increases, these LAGBs transform to HAGBs, corresponding to a “soft” dislocation structure. This may lead to a stable saturation flow stress of the material or to its softening. Their reported results for MDF in channel dies of aluminum 1050 with a strain amplitude $\Delta\varepsilon \approx 0.78$ shows a softening of the material after a cumulative deformation $\varepsilon \approx 5$. The results obtained by the present authors, for MDF of annealed copper[56] with strain amplitudes $\Delta\varepsilon$ ranging from 0.075 to 0.30 did not display softening. The interposition of LSA-MDF cycles between ECAP processing of aluminum and subsequent monotonic compression, as discussed in the present paper, initially raises the HAGBs fraction above the levels expected for processing only with ECAP and induced softening in the material. Subsequent monotonic compression started from a dislocation structure with an “excess” HAGBs fraction, displaying an anomalous quasi-linear work hardening.

No report in the literature was found regarding the microstructural evolution in the material caused by LSA-MDF after ECAP and for compression after ECAP+LSA-MDF. However, the present results bear some similarities to those from Armstrong for the application of LSA-MDF ($\Delta\varepsilon \approx 0.075$, total strain $\varepsilon \approx 4.2$) cycles to aluminum after an initial monotonic uniaxial compression ($\varepsilon \approx 1.6$)[32], causing a softening from ≈ 186 MPa down to ≈ 124 MPa. Table 2 displays the microstructural characteristics reported for this procedure. It should be remembered, however, that in the present experiments the initial straining was performed through 1 and 4ECAP passes with strain amplitude ≈ 1.15 per pass, following route Bc (total strain $\varepsilon \approx 1.15$ and 4.6, respectively). The resulting microstructures are different from those after initial monotonic compression (as utilized by Armstrong et al.[32]), due to the changes in the prevailing shearing plane in ECAP as the specimen is rotated around its axis in the Bc route. ECAP leads to frequent shear microbands intersections, resulting in different grain/subgrain/cells structures from those stemming from monotonic compression

Table 2. Microstructural characteristics reported by Armstrong et al.[32] for commercial purity aluminum submitted to Compression + LSA-MDF or LSA-MDF + Compression.

	Compression $\varepsilon = 1.6$	Compression $\varepsilon = 1.6$ + LSA-MDF, $\varepsilon = 4.2$, $\Delta\varepsilon = 0.075$
Subgrain size (μm)	1.8	1.9
Subgrain disorientation (º)	5.8	5.5
Cell size(μm)	0.75	0.90
Tangled dislocation area	0.16	0.08
Cells/subgrain	4.9	2.3
Subgrain/μm²	0.16	0.19
Cells/μm²	0.79	0.43

The data in Table 2 reports disorientations slightly above 5º for subgrains and cells; the latter would presumably have disorientations below 5º. One could thus consider that these subgrains and cells would correspond roughly to LAGBs (2-5º). Anyway, the application of LSA-MDF causes a decrease in the number of cells/subgrain from 4.9 to 2.3 and of the number of cells/μm² from 0.79 to 0.43, as well as a decrease in the tangled dislocation area from 0.16 to 0.08. This is similar to the tendencies described in Figure 8, where the application of LSA-MDF after ECAP causes a decrease in the fraction of LAGBs (2-5º).

3.3. Grain size and disorientation

Table 3 lists the grain (boundary disorientations > 15º) and cell sizes (boundary disorientations > 2º) for all the experimental conditions covered in this research.

Table 4 lists the average grain disorientations for all the experimental conditions covered in this research.

The grain size of aluminum after 4ECAP passes reported in Table 3 (1.64 μm) is similar to values reported in the literature[3,8,57] and to the value reported for the subgrain size for compression with a total strain $\varepsilon \approx 1.6$ in Table 4. The subgrain size in Table 3 (0.82 μm) is similar to the cell size after compression to 1.6 in Table 2. There is a remarkable difference in the total applied strain for the data in Tables 2 and 3 ($\varepsilon \approx 1.6$ and $\varepsilon \approx 4.6$ respectively); it seems that there is a structure size stabilization at relatively low values of total strain. The application of LSA-MDF after 4ECAP led to an initial decrease in the grain and cell sizes followed by its stabilization; the relationship grain size/cell size drops from ≈ 2 to ≈ 1.5. According to data in Table 2, compression + LSA-MDF leads to a small increase in subgrain size and a more pronounced increase in the cell size, as well to a drop in the relationship subgrain/cell size. Results from the present investigation and from that by Armstrong et al.[32] display the same microstructural tendencies.

Table 3 indicates that compression after 4ECAP and after 4ECAP+LSA-MDF increased both grain and cell sizes; similar results have been reported for compression with a total strain $\varepsilon \approx 1.3$ after ECAP[20]: the grain size rose

Table 3. Grain (boundary disorientations > 15º) and cell (boundary disorientations 2º a 15º) sizes for all experimental conditions in the present research.

	4ECAP	4ECAP+ 4LSA-MDF	4ECAP+ 8LSA-MDF	4ECAP+ 12LSA-MDF	4ECAP+ 16LSA-MDF
Grain size (μm)	1.64	1.26	1.77	1.87	1.74
Cell size(μm)	0.82	0.77	1.17	1.31	1.18
	4ECAP+COMP	**4ECAP+4LSA-MDF+COMP**	**4ECAP+8LSA-MDF+COMP**	**4ECAP+12LSA-MDF+COMP**	**4ECAP+16LSA-MDF+COMP**
Grain size (μm)	2.71	2.28	2.46	2.05	2.08
Cell size (μm)	1.43	1.10	1.32	1.38	1.24

Table 4. Average grain disorientation for all experimental conditions in the present research.

Average Disorientation (º)			
4ECAP	25	4ECAP+COMP	20
4ECAP+4MAC	30	4ECAP+4MAC+COMP	25
4ECAP+8MAC	30	4ECAP+8MAC+COMP	22
4ECAP+12MAC	31	4ECAP+12MAC+COMP	20
4ECAP+16MAC	30	4ECAP+16MAC+COMP	24

from 1.1 μm after ECAP to 1.95 μm after the compression. These authors also report that the compression after ECAP decreased the average grain orientation from 26º to 15º. The situation is again similar to the present results, as reported in Table 2: the initial average grain disorientation after 4ECAP was 25º, which fell to 20º after a compression with total strain $\varepsilon \approx 0.8$. The application of LSA-MDF raised the average disorientation of the grains in ECAP to ≈ 30º, but compression after 4ECAP + LSA-MDF always decreased the average grain disorientation.

It is suggested that the increase in grain and cell sizes caused by compression after 4ECAP and 4ECAP+LSA-MDF indicated in Table 3 is associated with the decrease of the average grain disorientation. Monotonic compression causes rotations in the grains, which would locally adopt orientations similar to adjacent grains and are thus considered as larger grains/cells under EBSD scanning. The examination of the larger grains in the EBSD OIMs in Figure 3 reveals that they contain small shades of color and isolated black lines, indicating that their orientation varies somewhat from region to region. It is noteworthy that a compression with $\varepsilon \approx 1.3$ after ECAP caused a more pronounced decrease in the average grain disorientation than a compression with total strain $\varepsilon \approx 0.8$ after ECAP + LSA-MDF; the increased monotonic compression strain would promote higher rotations of the grains.

According to data in Table 3, LSA-MDF causes some initial grain refinement followed by an increase and stabilization to a grain size somewhat above the initial grain size. On the other hand, the cell size displays an appreciable growth as the number of LSA-MDF cycles rises. The softening undergone by the material caused by the application of LSA-MDF cycles after 1 and 4ECAP can be partly connected to this cell growth and the corresponding Hall-Petch grain size effect. On the other hand, the increase of both grain and cell size caused by compression after ECAP and ECAP+LSA-MDF indicated in Table 3 should soften the material but this is not observed and actually a quasi-linear work hardening behavior is exhibited. This paradox is explained through a simultaneous increase in the presence of free dislocations inside the grains and LAGBs, overshadowing the grain size effect. Such free dislocation areas can be observed in the TEM images in Figure 5, especially in Figure 5j (examples are indicated by black arrows). It is noteworthy that Armstrong et al.[32] report that monotonic compression after MDF (strain amplitude $\Delta\varepsilon \approx 0.25$ up to a total strain $\varepsilon \approx 4.0$) displays a fraction of tangled dislocation area of 0.12; the same area, for only an initial MDF ($\Delta\varepsilon \approx 0.095$ up to a total strain $\varepsilon \approx 3.2$) exhibits a fraction of tangled dislocation area of only 0.04. Compression after LSA-MDF raises appreciably the area fraction with tangled dislocations.

An important area being developed in the SPD of metals is the so called "grain boundary engineering" or "grain boundary design"[9], where the presence and quantity of boundaries with specific characteristics are developed in order to reach desired functional properties. The capacity of LSA-MDF to change the fractions of the various types of grain boundaries generated by SPD, as demonstrated in the present investigation, makes this procedure an important tool for such grain boundary engineering. It should also be remembered that the size of the basic structural unit in cyclic HPT, and presumably also in MDF, can be modified by variations in strain amplitude ($\Delta\varepsilon$)[13], adding another tool for the grain boundary/structure design.

5. Conclusions

Simple compression after 4ECAP passes of aluminum following route Bc leads to an initial limited softening of the material followed by a limited work hardening. Rising numbers of Low Strain Amplitude MDF (LSA-MDF) cycles (strain amplitude $\Delta\varepsilon \approx 0.075$) applied after severe plastic deformation originated from 4ECAP passes following route Bc cause a softening of the material with a decreasing rate, coupled to a regeneration of the work-hardening rate of the material under subsequent simple compression, that rises almost linearly with the increasing number of LSA-MDF cycles.

Finite element simulations of plane strain compression of the material for the various work hardening rates measured in the present investigation show that the positive work hardening of the material in compression resulting from the application of LSA-MDF cycles after 4ECAP passes remarkably alleviates flow localization problems in the plane strain post SPD forming of aluminum under plane strain conditions. LSA-MDF after ECAP is an important technique in order to circumvent work softening effects in the post SPD forming of aluminum.

The initial softening caused by increasing numbers of LSA-MDF cycles after 4ECAP passes is associated with a rise in the fraction of HABGs in the material followed by its stabilization; further softening is attributed to an increase in the boundary disorientations in the LAGBs, whose fractions decrease for the range of 2–5º and increase for the range 5–15º. In addition, an appreciable increase in the cell sizes is observed, also contributing to the material softening.

The positive work hardening rates in the monotonic compression after ECAP+LSA-MDF is connected to decreases in the fraction of HAGBs in the material, increases the fraction of LAGBs, especially in the range from 2–5º, and in the area fraction displaying tangled dislocations.

Monotonic compression causes an increase in the grain and cell sizes of the material that should lead to softening and not hardening of the material. These size effects seem to be overshadowed by the changes in dislocation arrangement.

Compression after 4ECAP+LSA-MDF decreases the average disorientation of the grains/cells; it is suggested this is caused by grain/cells rotations during monotonic compression, leading to local mergers of regions initially displaying low disorientations.

6. Acknowledgments

This study was financed by CNPq (National Council for Research and Technological Development, Grant 300874/2018-9 and 301758/2022-0), Fundação de Amparo à Pesquisa de Minas Gerais (FAPEMIG) Grant APQ-01208-21 and the Coordenação de Aperfeiçoamento de Pessoal de Nível Superior - Brasil (CAPES, Finance Code 001). The authors thank SIXPRO V. P. P. for the permission of use of QForm software for the computer simulations and to Pedro Henrique Silva for help in these simulations.

7. References

1. Valiev RZ, Estrin Y, Horita Z, Langdon TG, Zehetbauer MJ, Zhu YT. Producing bulk ultrafine-grained materials by severe plastic deformation. J Met. 2006;58:33-9.
2. Valiev RZ, Estrin Y, Horita Z, Langdon TG, Zehetbauer MJ, Zhu YT. Fundamentals of superior properties in bulk nanoSPD materials. Mater Res Lett. 2016;4:1-21.
3. El-Danaf EA. Mechanical properties and microstructure evolution of 1050 aluminum severely deformed by ECAP to 16 passes. Mater Sci Eng A. 2008;487(1-2):189-200.
4. Edalati K, Bachmaier A, Beloshenko VA, Bygelzimer Y, Blank VD, Botta WJ, et al. Nanomaterials by severe plastic deformation: review of historical developments and recent advances. Mater Res Lett. 2022;10(4):163-256.
5. Sabirov I, Murashkin MY, Valiev RZ. Nanostructured aluminium alloys produced by severe plastic deformation: new horizons in development. Mater Sci Eng A. 2013;560:1-24.
6. Sakai T, Belyakova A, Kibishev R, Miura H, Jonas JJ. Dynamic and post-dynamic recrystallization under hot, cold and severe plastic deformation conditions. Prog Mater Sci. 2014;60:130-207.
7. Zhilyaev AP, Langdon TG. Using high-pressure torsion for metal processing: fundamentals and applications. Prog Mater Sci. 2008;53(6):893-979.
8. Tejedor R, Edalati K, Benito JA, Horita Z, Cabrera JM. High-pressure torsion of iron with various purity levels and validation of Hall-Petch strengthening mechanism. Mater Sci Eng A. 2019;743:597-605.
9. Valiev RZ, Langdon TG. Principles of equal-channel angular pressing as a processing tool for grain refinement. Prog Mater Sci. 2006;51:881-981.
10. Valiev RZ, Islamgaliev RK, Alexandrov IV. Bulk nanostructured materials from severe plastic deformation. Prog Mater Sci. 2000;45:103-89.
11. Estrin Y, Vinogradov A. Extreme grain refinement by severe plastic deformation: a wealth of challenging science. Acta Mater. 2013;61:782-817.
12. Xu X, Zhang Q, Hu N, Huang Y, Langdon TG. Using an Al–Cu binary alloy to compare processing by multi-axial compression and high-pressure torsion. Mater Sci Eng A. 2013;588:280-7.
13. Wetscher F, Pippan R. Cyclic high pressure torsion of nickel and Armco iron. Philos Mag. 2006;86:867-5883.
14. Langdon TG. Twenty-five years of ultrafine-grained materials: achieving exceptional properties through grain refinement. Acta Mater. 2013;61:7035-59.
15. Sakai T, Miura H, Yang X. Ultrafine grain formation in face centered cubic metals during severe plastic deformation. Mater Sci Eng A. 2009;499:2-6.
16. Guo W, Wang Q, Ye B, Zhou H. Microstructure and mechanical properties of AZ31 magnesium alloy processed by cyclic closed-die forging. J Alloys Compd. 2013;558:164-71.
17. Flausino PCA, Nassif MEL, De Castro BF, Pereira PHR, Aguilar MTP, Cetlin PR. Microstructural evolution and mechanical behavior of copper processed by low strain amplitude multi-directional forging. Mater Sci Eng A. 2019;756:474-83.
18. Almeida NGS, Pereira PHR, De Faria CG, Aguilar MTP, Cetlin PR. Mechanical behavior and microstructures of aluminum processed by low strain amplitude multi-directional confined forging. J Mater Res Technol. 2020;9(3):3190-7.
19. Beyerlein IJ, Alexander DJ, Tomé CN. Plastic anisotropy in aluminum and copper pre-strained by Equal Channel angular extrusion. J Mater Sci. 2007;42:1733-50.
20. El-Danaf EA, Soliman MS, Almajid AS, El-Rayes MM. Enhancement of mechanical properties and grain size refinement of commercial purity aluminum 1050 processed by ECAP. Mater Sci Eng A. 2007;458:226-34.
21. Backofen WA. Deformation processing. Reading: Addison Wesley; 1972. p. 253-56.
22. Semiatin SL, Jonas JJ. Formability & workability of metals: plastic instability and flow localization. Metals Park, Ohio: American Society for Metals; 1984. p. 69-71.
23. May J, Höppel HW, Göken M. Strain rate sensitivity of ultrafine grained aluminum processed by severe plastic deformation. Scr Mater. 2005;53:189-94.
24. El-Danaf EA. Mechanical properties, microstructure and texture of single pass equal channel angular pressed 1050, 5083, 6082 and 7010 aluminum alloys with different dies. Mater Des. 2011;32:3838-53.
25. Figueiredo RB, Aguilar MTP, Cetlin PR. Finite element modelling of plastic instability during ecap processing of flow-softening metals. Mater Sci Eng A. 2006;430:179-84.
26. Fan GJ, Choo H, Liaw PK, Lavernia EJ. Plastic deformation and fracture of ultrafine-grained Al–Mg alloys with a bimodal grain size distribution. Acta Mater. 2006;54:1759-66.
27. Han BQ, Huang JY, Zhu EJ, Lavernia EJ. Strain rate dependence of properties of cryomilled bimodal 5083 Al alloys. Acta Mater. 2006;54:3015-24.
28. Wang Y, Chen M, Zhou F, Ma E. High tensile ductility in a nanostructured metal. Nature. 2002;419:912-5.
29. Cheng S, Zhao YT, Zhu E. Optimizing the strength and ductility of fine structured 2024 Al alloy by nano-precipitation. Acta Mater. 2007;55:5822-32.
30. Hockauf M, Meyer LW, Zillman B, Hietschold M, Schultze S, Krueger L. Simultaneous improvement of strength and ductility of Al–Mg–Si alloys by combining equal-channel angular extrusion with subsequent high-temperature short-time aging. Mater Sci Eng A. 2009;503:167-71.
31. Valiev RZ, Murashkin MY, Kilmametov A, Straumal B, Chinh NQ, Langdon TG. Unusual super-ductility at room temperature in an ultrafine-grained aluminum alloy. J Mater Sci. 2010;45(17):4718-24.
32. Armstrong PE, Hockett JE, Sherby OD. Large strain multidirectional deformation of 1100 aluminum at 300 K. J Mech Phys Solids. 1982;30(1-2):37-58.
33. De Faria CG, Almeida NGS, Aguilar MTP, Cetlin PR. Increasing the work hardening capacity of equal channel angular pressed (ECAPed) aluminum through multi-axial compression (MAC). Mater Lett. 2016;174:153-6.
34. De Faria CG, Almeida NGS, Balzuweit K, Aguilar MTP, Cetlin PR. The effect of initial strain in the severe plastic deformation of aluminum on the subsequent work hardening regeneration through Low Strain Amplitude Multi-Directional Forging. Mater Lett. 2021;290:129462.
35. Coffin LF, Tavernelli JF. The cyclic straining and fatigue of metals. Trans Metall Soc AIME. 1959;215:794-806.
36. Pinheiro IP, Barbosa RANM, Cetlin PR. Dynamic restoration during the hot cyclic straining of copper. Scr Mater. 1998;38(1):53-7.
37. Pinheiro IP, Barbosa RANM, Cetlin PR. Effect of the cyclic strain amplitude on the hot dynamic restoration of copper. Scr Mater. 2001;44(1):187-93.
38. Pinheiro IP, Barbosa RANM, Cetlin PR. The effect of cyclic torsion on the hot dynamic restoration of interstitial free steel in the austenitic range. J Mater Process Technol. 2002;125:125-9.

39. Pinheiro IP, Barbosa RANM, Cetlin PR. The mechanical behaviour and microstructures of interstitial free steel strained in monotonic or cyclic torsion at 1223K. ISIJ Int. 2006;46(5):734-43.
40. Ito Y, Edalati K, Horita Z. High pressure torsion of aluminum with ultra-high purity (99.9999%) and occurrence of inverse Hall-Petch relationship. Mater Sci Eng A. 2017;679:428-34.
41. Mazilkin AA, Straumal BB, Rabkin E, Baretzy B, Enders S, Protasova SG, et al. Softening of nanostructured Al-Zn and Al-Mg alloys after severe plastic deformation. Acta Mater. 2006;54:3933-9.
42. Da Silva NAN, Pereira PHR, Corrêa ECS, Aguilar MTP, Cetlin PR. Microstructural evolution and mechanical properties in a Zn–Al–Cu–Mg hypoeutectic alloy processed by multi-directional forging at room temperature. Mater Sci Eng A. 2020;801:140420.
43. Kapoor R, Sarkar A, Yogi R, Shekhawat SK, Samajdar I, Chakravartty JK. Softening of Al during multi-axial forging in a channel die. Mater Sci Eng A. 2013;560:404-12.
44. Muñoz JA, Bolmaro RE, Jorge AM Jr, Zhilyaev A, Cabrera JM. Prediction of the generation of High- and Low-angle grain boundaries (HAGB and LAGB) during Severe Plastic Deformation. Metall Mater Trans, A Phys Metall Mater Sci. 2020;51:4674-84. http://doi.org/10.1007/s11661-020-05873-3.
45. De Faria CG, Almeida NGS, Balzuweit K, Aguilar MTP, Cetlin PR. The effect of initial strain in the severe plastic deformation of aluminum on the subsequent work hardening regeneration through Low Strain Amplitude Multi-Directional Forging. Mater Lett. 2021;290:129462.
46. De Faria CG, Almeida NGS, Bubani FDC, Balzuweit K, Aguilar MTP, Cetlin PR. Microstructural evolution in the low strain amplitude multi-axial compression (LSA-MAC) after equal channel equal pressing (ECAP) of aluminum. Mater Lett. 2018;227:149-53.
47. El Aal MIA, Um HY, Yoon EY, Kim HS. Microstructure evolution and mechanical properties of pure aluminum deformed by equal channel angular pressing and direct extrusion in one step through an integrated die. Mater Sci Eng A. 2015;625:252-63.
48. Zhang Z, Wang J, Zhang Q, Zhang S, Shi Q, Qi H. Research on Grain refinement mechanism of 6061 Aluminum alloy processed by combined SPD methods of ECAP and MAC. Materials (Basel). 2008;11:1246.
49. Iwahashi Y, Horita Z, Nemoto M, Langdon TG. Principle of equal-channel angular pressing for the processing of ultra-fine grained materials. Scr Mater. 1996;35:143-6.
50. Iwahashi Y, Horita Z, Nemoto M, Langdon TG. The process of grain refinement in Equal-Channel Angular Pressing. Acta Mater. 1998;46:3317-31.
51. Beausir B, Fundenberger JJ. Analysis Tools for Electron and X-ray Diffraction, ATEX – Software. Metz: Université de Lorraine; 2017 [cited 2023 Oct 16]. Available from: www.atex-software.eu
52. Backofen WA. Deformation processing. Reading: Addison Wesley; 1972. Chapter 7.
53. Coffin LF, Tavernelli JF. The cyclic straining and fatigue of metals. Trans Metall Soc AIME. 1959;215:794-806.
54. Sakai T, Jonas JJ. Overview no. 35 dynamic recrystallization: mechanical and microstructural considerations. Acta Metall. 1984;32:189-209.
55. Sabbaghianrad S, Kawasaki M, Langdon TG. Microstructural evolution and the mechanical properties of an aluminum alloy processed by high-pressure torsion. J Mater Sci. 2012;47:7789-95.
56. Flausino PCA, Nassif MEL, Bubani FDC, Pereira PHR, Aguilar MTP, Cetlin PR. Influence of strain amplitude on the microstructural evolution and flow properties of Copper processed by Multidirectional Forging. Adv Eng Mater. 2020;22:1901510.
57. Furukawa M, Horita Z, Nemoto M, Langdon TG. The use of severe plastic deformation for microstructural control. Mater Sci Eng A. 2022;324(1-2):82-9.